

Flatness-based Finite-Horizon Multi-UAV Formation Trajectory Planning and Directionally Aware Collision Avoidance Tracking

Hossein B. Jond¹, Logan Beaver², Martin Jiroušek¹, Naiemeh Ahmadrlo³, Veli Bakircioğlu^{1,4}, and Martin Saska¹

¹Department of Cybernetics, Czech Technical University in Prague, Prague, Czechia

²Mechanical and Aerospace Engineering, Old Dominion University, Norfolk, VA, USA

³Mechanical Engineering Faculty, Sahand University of Technology, New Sahand Town, Tabriz, Iran

⁴Aksaray University, Aksaray, Türkiye

July 1, 2025

Abstract

Collision-free optimal formation control of unmanned aerial vehicle (UAV) teams is challenging. The state-of-the-art optimal control approaches often rely on numerical methods sensitive to initial guesses. This paper presents an innovative collision-free finite-time formation control scheme for multiple UAVs leveraging the differential flatness of the UAV dynamics, eliminating the need for numerical methods. We formulate a finite-time optimal control problem to plan a formation trajectory for feasible initial states. This formation trajectory planning optimal control problem involves a collective performance index to meet the formation requirements of achieving relative positions and velocity consensus. It is solved by applying Pontryagin's principle. Subsequently, a collision-constrained regulating problem is addressed to ensure collision-free tracking of the planned formation trajectory. The tracking problem incorporates a directionally aware collision avoidance strategy that prioritizes avoiding UAVs in the forward path and relative approach. It assigns lower priority to those on the sides with an oblique relative approach and disregards UAVs behind and not in the relative approach. The simulation results for a four-UAV team (re)formation problem confirm the efficacy of the proposed control scheme.

Keywords: Differential flatness; Formation control; Pontryagin's principle

1 Introduction

Formation control of unmanned aerial vehicles (UAVs) has received growing interest in recent decades with a broad range of applications in exploring hazardous terrain [1], transporting loads [2],

performing perilous inspection tasks [3], surveying structures of historical significance [4], and more. In formation trajectory planning, UAVs plan optimal or sub-optimal collision-free trajectories between their initial and terminal states [5, 6]. In formation trajectory tracking, all UAVs converge to the pre-planned formation trajectories [7, 8, 9].

The nonlinear dynamics of UAVs, inter-UAV collision-free coordination, and UAV-obstacle collision avoidance pose additional challenges to formation trajectory planning and tracking. Finite-horizon formation control, achievable by optimizing a collective performance index consisting of UAV states and control inputs within a finite time frame, holds practical significance [10]. The time frame is constrained when UAV groups plan to create a formation to execute maneuvers, reach destinations, optimize resource utilization (e.g., energy), and, most importantly, ensure adherence to safety constraints. Consequently, collision-free finite-time formation trajectory planning and tracking are a frontier of ongoing research.

Optimal trajectory planning for UAV systems is difficult, and solutions often rely on numerical methods that can be sensitive to initial guesses [11]. Instead, most studies on formation trajectory planning focus on either interpolating or approximating the optimal trajectories between the initial and terminal states [12]. In [12, 5], algorithms are developed for generating collision-free finite-time trajectories for multi-UAV systems, utilizing Bézier curves [12], high-order piecewise polynomials [5], and piecewise polynomial trajectory generation for UAVs recursively [6] to parameterize trajectories between the initial and terminal states. However, the literature on UAV formation control lacks approaches for collision-avoidance finite-horizon formation trajectory planning and tracking of UAVs solely based on their initial states.

This paper leverages the inherent differential flatness property of quadrotor-type UAV dynamics to introduce a finite-horizon formation trajectory planning and tracking control scheme solely based on UAVs' initial states. The finite-horizon planning trajectories in the flat coordinates are derived by applying necessary and sufficient conditions for optimality using Pontryagin's principle. The trajectory tracking control system is optimal when all UAVs operate within their safety region and becomes sub-optimal when any two UAVs enter their collision reaction region. The paper's main contribution is an inter-UAV collision-free optimal finite-horizon formation control scheme for formation trajectory planning and tracking using solely the initial state of UAVs. The proposed approach

1. is consensus-based and, unlike [13, 14, 15, 16], does not rely on a (virtual or actual) leader, which typically serves as the external reference for the formation, thereby enhancing robustness and scalability by eliminating potential single-point failures,
2. unlike [12, 5, 6], solely uses the initial states of the UAVs to plan optimal trajectories, which reduces computational complexity and eliminates the need for external references or predefined waypoints,
3. unlike [16], employs a finite horizon, which enables real-time adaptability to changing tasks and dynamic environments with finite time convergence, and
4. finally, introduces a directionally aware collision avoidance strategy that prioritizes collision avoidance both in the forward path and the relative approach for each UAV. This results in an adaptive and efficient behavior that reduces or prevents unnecessary maneuvering toward UAVs on the sides or behind, as well as those not on a relative approach trajectory, which are less likely to pose an immediate threat or pose no threat. This aspect is not addressed in existing works such as [8, 17].

The rest of this paper is organized as follows. Section 2 provides preliminaries. The collision-free finite-time formation control is defined in Section 3. Section 4 recasts the problem definition as optimal control problems where their solution is investigated. The directionally aware collision avoidance strategy is introduced in Section 5. Section 6 illustrates the simulation results for a four-UAV team (re)formation. Section 7 concludes the paper.

2 Preliminaries

2.1 graph theory

A directed graph is a pair $\mathcal{G}(\mathcal{V}, \mathcal{E})$ where \mathcal{V} is a finite set of vertices/nodes and $\mathcal{E} \subseteq \{(i, j) : i, j \in \mathcal{V}\}$ is a set of directed edges/arcs. Each edge $(i, j) \in \mathcal{E}$ represents a directional information flow and is assigned with a positive scalar weight $\mu_{ij} > 0$. An undirected graph is similarly defined with its edges being undirected, indicating bidirectional information flow. Graph \mathcal{G} is connected meaning that for every pair of vertices $(i, j) \in \mathcal{V} \times \mathcal{V}$, from i to j for all $j \in \mathcal{V}, j \neq i$, there exists a path of (undirected) edges from \mathcal{E} .

The graph Laplacian matrix is defined as

$$\mathbf{L} = \mathbf{D}\mathbf{W}\mathbf{D}^\top \in \mathbb{R}^N.$$

Matrix $\mathbf{D} \in \mathbb{R}^{|\mathcal{V}| \times |\mathcal{E}|}$ is the incidence matrix of \mathcal{G} where \mathbf{D} 's ij th element is 1 if the node i is the tail of the edge j , -1 if the node i is the head, and 0, otherwise. For an undirected graph, the designation of the tail or head is arbitrary. Matrix $\mathbf{W} = \text{diag}(\dots, \mu_{ij}, \dots) \forall (i, j) \in \mathcal{E} \in \mathbb{R}^{|\mathcal{E}|}$. Matrix \mathbf{L} is symmetric ($\mathbf{L} = \mathbf{L}^\top$), positive semidefinite (PSD) ($\mathbf{L} \succeq \mathbf{0}$), and satisfies the sum-of-squares property

$$\sum_{(i,j) \in \mathcal{E}} \mu_{ij} \|\mathbf{x}_i - \mathbf{x}_j\|^2 = \mathbf{x}^\top (\mathbf{L} \otimes \mathbf{I}_m) \mathbf{x}, \quad (1)$$

where $\mathbf{x} = [\mathbf{x}_1^\top, \dots, \mathbf{x}_N^\top]^\top \in \mathbb{R}^{mN}$, $\mathbf{x}_i \in \mathbb{R}^m$, $\mathbf{I}_m \in \mathbb{R}^m$ is the identity matrix of dimension m , \otimes demonstrates the Kronecker product operator, and $\|\cdot\|$ is the Euclidean norm.

Let $\mathbf{Y} = [y_{ij}] \in \mathbb{R}^{p \times q}$. Thus,

$$\mathbf{Y} \otimes \mathbf{I}_m = \begin{bmatrix} y_{11}\mathbf{I}_m & \cdots & y_{1q}\mathbf{I}_m \\ \vdots & \ddots & \vdots \\ y_{p1}\mathbf{I}_m & \cdots & y_{pq}\mathbf{I}_m \end{bmatrix} \in \mathbb{R}^{mp \times mq}.$$

2.2 UAV model

The UAV model is a quadrotor consisting of a rigid cross frame with four rotors, as depicted in Fig. 1. The equations of motion governing the acceleration of the center of mass for a quadrotor UAV indexed by i are given as follows [18]

$$m\ddot{\mathbf{p}}_i(t) = -mg\mathbf{z}_W + u_{i1}(t)\mathbf{z}_B, \quad (2)$$

$$\dot{\boldsymbol{\omega}}_{B\mathcal{W}}(t) = \mathcal{I}^{-1} \{ -\boldsymbol{\omega}_{B\mathcal{W}}(t) \times \mathcal{I}\boldsymbol{\omega}_{B\mathcal{W}}(t) + [u_{i2}(t) \quad u_{i3}(t) \quad u_{i4}(t)]^\top \}, \quad (3)$$

where $\mathbf{p}_i(t) = [x_i(t), y_i(t), z_i(t)]^\top \in \mathbb{R}^3$ is the position vector of the center of mass in the world frame \mathcal{W} , $\boldsymbol{\omega}_{B\mathcal{W}}(t)$ is the angular velocity of the body frame \mathcal{B} relative to the world frame \mathcal{W} , \mathcal{I}

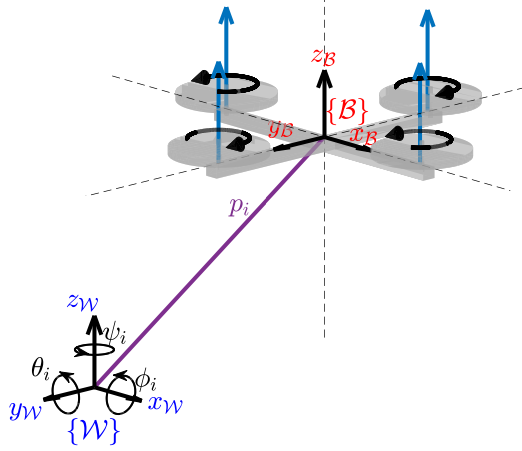


Figure 1: Quadrotor configuration. \mathcal{W} and \mathcal{B} denote the world frame and body frame, respectively. The roll, pitch, and yaw angles of the vehicle are denoted by $\phi_i(t)$, $\theta_i(t)$, and $\psi_i(t)$, respectively.

is the moment of inertia matrix referenced to the center of mass along the body axes $\mathbf{x}_B, \mathbf{y}_B, \mathbf{z}_B$, m is the mass of the quadrotor, and g is the gravitational acceleration. The control input to the quadrotor is $\mathbf{u}_i(t) \in \mathbb{R}^4$ where $u_{i1}(t)$ is the net body force and $u_{i2}(t), u_{i3}(t), u_{i4}(t)$ are the body moments which can be expressed according to the rotor speeds.

3 Problem definition

Consider a multi-UAV team of N quadrotors indexed by $\mathcal{V} = \{1, \dots, N\}$. Each UAV $i \in \mathcal{V}$ is described by the dynamics (2)–(3). Two time-invariant connected directed graphs are defined: the formation graph $\mathcal{G}_f(\mathcal{V}, \mathcal{E}_f)$ and the communication graph $\mathcal{G}_c(\mathcal{V}, \mathcal{E}_c)$. The formation graph specifies the desired spatial formation shape, while the communication graph outlines the inter-UAV communications.

Assumption 1. *The formation graph is connected.*

Assumption 2. *The communication graph is complete to account for all inter-UAV collisions (thus, $\mathcal{G}_f \subseteq \mathcal{G}_c$).*

The collision-free formation control problem consists of steering all UAVs from their initial state to a desired formation while avoiding inter-UAV collisions. Formation shape is determined by the offset vectors $\mathbf{d}_{ij} \in \mathbb{R}^3$ for all UAV pairs $(i, j) \in \mathcal{E}_f$. Each UAV $i \in \mathcal{V}$ has an avoidance region radius r_i , meaning the minimum safe distance between two UAVs i and j is $r_i + r_j$. Let R_i denote the radius of the collision reaction region of each UAV $i \in \mathcal{V}$ and $R_i > r_i$ (see Fig. 2).

Define the UAV team position vector $\mathbf{p}(t) = [\mathbf{p}_1^\top(t), \dots, \mathbf{p}_N^\top(t)]^\top \in \mathbb{R}^{3N}$. The following regions are defined accordingly

1. safety region: $\Psi(\mathbf{p}) \triangleq \{\mathbf{p}(t) | \mathbf{p}_i(t) \in \mathbb{R}^3, \|\mathbf{p}_i(t) - \mathbf{p}_j(t)\| \geq R_i + R_j, \forall (i, j) \in \mathcal{E}_c\}$,
2. collision reaction region: $\Gamma(\mathbf{p}) \triangleq \{\mathbf{p}(t) | \mathbf{p}_i(t) \in \mathbb{R}^3, r_i + r_j < \|\mathbf{p}_i(t) - \mathbf{p}_j(t)\| < R_i + R_j, \exists (i, j) \in \mathcal{E}_c\}$, and

3. collision region: $\Lambda(\mathbf{p}) \triangleq \{\mathbf{p}(t) | \mathbf{p}_i(t) \in \mathbb{R}^3, \|\mathbf{p}_i(t) - \mathbf{p}_j(t)\| < r_i + r_j, \exists(i, j) \in \mathcal{E}_c\}$,
4. singularity: $\Phi(\mathbf{p}) \triangleq \{\mathbf{p}(t) | \mathbf{p}_i(t) \in \mathbb{R}^3, \|\mathbf{p}_i(t) - \mathbf{p}_j(t)\| = r_i + r_j, \exists(i, j) \in \mathcal{E}_c\}$.

We make the following assumption.

Assumption 3. $\Lambda(\mathbf{p}(0)) = \Phi(\mathbf{p}(0)) = \Lambda(\mathbf{p}(t_f)) = \Phi(\mathbf{p}(t_f)) = \emptyset$.

The multi-UAV formation control problem is defined as follows.

Problem 1. (a) Consider a multi-UAV system on the directed connected graph $\mathcal{G}_f(\mathcal{V}, \mathcal{E}_f)$ with UAV dynamics (2)–(3). The multi-UAV formation control problem is to determine control strategies that drive all UAVs from their initial state to a desired formation specified by $\mathbf{d}_{ij}, \forall(i, j) \in \mathcal{E}_f$ in the state space in a finite time horizon $t_f > 0$. (b) All UAVs must avoid mutual collisions, i.e., $\Lambda(\mathbf{p})$ and $\Phi(\mathbf{p})$ must be \emptyset for all $t \in (0, t_f)$.

The formation control objective is to ensure

$$\sum_{(i,j) \in \mathcal{E}_f} \{\|\mathbf{p}_i(t) - \mathbf{p}_j(t) - \mathbf{d}_{ij}\|^2 + \|\dot{\mathbf{p}}_i(t) - \dot{\mathbf{p}}_j(t)\|^2\} \rightarrow 0, \text{ as } t \rightarrow t_f, \quad (4)$$

for any initial position $\mathbf{p}_i(0)$ and velocity $\dot{\mathbf{p}}_i(0)$ with $i \in \mathcal{V}$ and while satisfying the collision avoidance constraint

$$\|\mathbf{p}_i(t) - \mathbf{p}_j(t)\| > r_i + r_j, \quad \forall(i, j) \in \mathcal{E}_c, \forall t \in (0, t_f). \quad (5)$$

The UAV dynamics, formation control objective, and collision avoidance constraint described by (2)–(5) can be recast as a constrained optimal control problem. This allows for investigating optimal formation control strategies for Problem 1. However, finding a solution is problematic due to the nonlinear UAV dynamics. Numerical methods can be sensitive to initialization [11] and unstable, often relegating them to a lower priority [19, 20]. Moreover, the quadrotor system is inherently underactuated, with six degrees of freedom but only four control inputs. This characteristic poses an additional challenge in finding a solution that adheres to the system’s underactuation dynamics.

In the next section, we present a collision-free formation trajectory planning and tracking scheme leveraging the differential flatness property of the UAV dynamics.

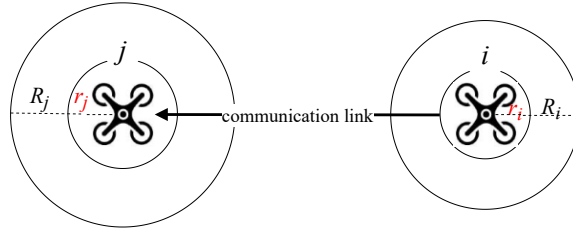


Figure 2: UAV workspace configuration showing the safe distance r_i and collision reaction distance R_i .

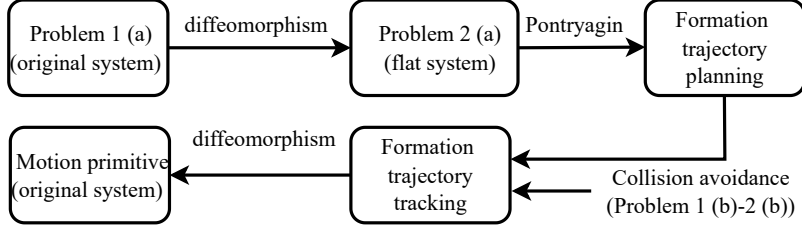


Figure 3: Outline of the control scheme for generating collision-free motion primitives for UAV formation. The formation trajectory planning signal is optimal. Subsequently, this trajectory is tracked within the safety region using an optimal tracking control law. The tracking law becomes sub-optimal in the collision reaction region, ensuring collision-free motion by sacrificing optimality.

4 Collision-Free Trajectory Planning and Tracking

Leveraging the differential flatness property of the UAV dynamics provides a fully actuated system with four flat outputs [18, 21, 22, 14]. By applying a diffeomorphism (see Definition 1 from [23]), Problem 1 is transformed into a flat space where it becomes easier to handle due to the linear UAV dynamics. The simplified problem, denoted as Problem 2, is recast and addressed as optimal control trajectory planning and tracking problems in flat space. The flat space control strategies are then transformed back to the original coordinate system using the inverse of the diffeomorphism. This approach is summarized in the control scheme diagram in Fig. 3.

4.1 optimal trajectories in flat coordinates

The flat output vector is defined as $\mathbf{z}_i(t) = [\mathbf{p}_i^\top(t), \psi_i(t)]^\top \in \mathbb{R}^4$ where $\mathbf{p}_i(t)$ is the coordinate of the center of mass of the i th UAV in the world coordinate system and $\psi_i(t)$ is its yaw angle. The flat input vector is $\ddot{\mathbf{z}}_i(t) \in \mathbb{R}^3$. The collective thrust $u_{i1}(t)$ exerted by the propellers of the i th quadrotor is directly determined by the flat outputs and their derivatives. Since angular velocity and acceleration are dependent on these outputs and their derivatives, (3) is employed to calculate the inputs $u_{i2}(t)$, $u_{i3}(t)$, and $u_{i4}(t)$ (see [18]).

Define $\boldsymbol{\psi}(t) = [\psi_1(t), \dots, \psi_N(t)]^\top \in \mathbb{R}^N$. The UAV team flat state and control input vectors are defined as $\mathbf{r}(t) = [\mathbf{p}^\top(t), \boldsymbol{\psi}^\top(t), \dot{\mathbf{p}}^\top(t), \dot{\boldsymbol{\psi}}^\top(t), \ddot{\mathbf{p}}^\top(t), \ddot{\boldsymbol{\psi}}^\top(t), 1]^\top \in \mathbb{R}^{12N+1}$ and $\mathbf{u}_r(t) = [\ddot{\mathbf{p}}(t), \ddot{\boldsymbol{\psi}}(t)]^\top \in \mathbb{R}^{4N}$, respectively. The multi-UAV team dynamics in flat space is given by

$$\dot{\mathbf{r}}(t) = \mathbf{A}\mathbf{r}(t) + \mathbf{B}\mathbf{u}_r(t), \quad \mathbf{r}(0) = \mathbf{r}_0, \quad (6)$$

where $\mathbf{A} = \begin{bmatrix} \mathbf{A}_0 & \mathbf{0} \\ \mathbf{0} & \mathbf{0} \end{bmatrix} \in \mathbb{R}^{12N+1}$, $\mathbf{A}_0 = \begin{bmatrix} 0 & 1 & 0 \\ 0 & 0 & 1 \\ 0 & 0 & 0 \end{bmatrix} \otimes \mathbf{I}_{4N}$, $\mathbf{B} = \begin{bmatrix} \mathbf{B}_0 \\ \mathbf{0} \end{bmatrix} \in \mathbb{R}^{(12N+1) \times 4N}$, and $\mathbf{B}_0 = \begin{bmatrix} 0 & 0 & 1 \end{bmatrix}^\top \otimes \mathbf{I}_{4N}$.

Problem 2. (a) Consider a multi-UAV system on the directed connected graph $\mathcal{G}_f(\mathcal{V}, \mathcal{E}_f)$ in flat space with dynamics (6). The multi-UAV formation control problem is to determine control strategies for the UAV team that drive all UAVs from their initial state to a desired formation specified by $\mathbf{d}_{ij}, \forall (i, j) \in \mathcal{E}_f$ in the flat state space in a finite time horizon t_f . (b) Additionally, $\Lambda(\mathbf{p})$ and $\Phi(\mathbf{p})$ must be \emptyset for all $t \in (0, t_f)$.

The formation control objective (4) and collision avoidance constraint (5) in the original coordinates are transferred unchanged to flat coordinates. *Problem 2* (a) pertains to an unconstrained control problem. In the following, we will first address *Problem 2* (a) for formation trajectory planning and then use the resulting trajectory in a collision-free tracking controller to solve *Problem 2* in its entirety (see Fig. 3).

Using the finite-time linear quadratic paradigm, *Problem 2* (a) is recast as the following optimal control problem

$$\min_{\mathbf{u}_r} C(\mathbf{r}(t_f)) + \int_0^{t_f} (L(\mathbf{r}(t)) + \mathbf{u}_r^\top(t) \mathbf{R} \mathbf{u}_r(t)) dt, \quad (7)$$

subject to state dynamics (6) where

$$C(\mathbf{r}(t_f)) = \sum_{(i,j) \in \mathcal{E}_f} \omega_{ij} (\|\mathbf{p}_i(t_f) - \mathbf{p}_j(t_f) - \mathbf{d}_{ij}\|^2 + \|\dot{\mathbf{p}}_i(t_f) - \dot{\mathbf{p}}_j(t_f)\|^2),$$

$$L(\mathbf{r}(t)) = \sum_{(i,j) \in \mathcal{E}_f} \mu_{ij} (\|\mathbf{p}_i(t) - \mathbf{p}_j(t) - \mathbf{d}_{ij}\|^2 + \|\dot{\mathbf{p}}_i(t) - \dot{\mathbf{p}}_j(t)\|^2),$$

$\omega_{ij} > 0$, $\mathbf{R} = \text{diag}(\gamma_1, \dots, \gamma_N) \otimes \mathbf{I}_4$, and $\gamma_i > 0$. The collective performance index (7) quadratically penalizes the UAV team's deviations from cooperative formation behavior (i.e., achieving relative distances and velocity consensus) while expending the least control effort.

Using the sum-of-squares property of graph Laplacian matrix in (1), the terminal and running formation error components in (7), respectively, are compacted as [24, 25]

$$C(\mathbf{r}(t_f)) = \mathbf{r}^\top(t_f) \mathbf{Q}_f \mathbf{r}(t_f), \quad L(\mathbf{z}(t)) = \mathbf{r}^\top(t) \mathbf{Q} \mathbf{r}(t),$$

where $\mathbf{Q}_f = \begin{bmatrix} \hat{\mathbf{L}}_f & \mathbf{0}_{4N} & \mathbf{0}_{4N} & -\boldsymbol{\Theta}_f \\ \mathbf{0}_{4N} & \hat{\mathbf{L}}_f & \mathbf{0}_{4N} & \mathbf{0}_{4N \times 1} \\ \mathbf{0}_{4N} & \mathbf{0}_{4N} & \mathbf{0}_{4N} & \mathbf{0}_{4N \times 1} \\ -\boldsymbol{\Theta}_f^\top & \mathbf{0}_{1 \times 4N} & \mathbf{0}_{1 \times 4N} & \boldsymbol{\Upsilon}_f \end{bmatrix} \in \mathbb{R}^{12N+1}$, $\mathbf{Q} = \begin{bmatrix} \hat{\mathbf{L}} & \mathbf{0}_{4N} & \mathbf{0}_{4N} & -\boldsymbol{\Theta} \\ \mathbf{0}_{4N} & \hat{\mathbf{L}} & \mathbf{0}_{4N} & \mathbf{0}_{4N \times 1} \\ \mathbf{0}_{4N} & \mathbf{0}_{4N} & \mathbf{0}_{4N} & \mathbf{0}_{4N \times 1} \\ -\boldsymbol{\Theta}^\top & \mathbf{0}_{1 \times 4N} & \mathbf{0}_{1 \times 4N} & \boldsymbol{\Upsilon} \end{bmatrix} \in \mathbb{R}^{12N+1}$, $\hat{\mathbf{L}}_f = \begin{bmatrix} \mathbf{L}_f \otimes \mathbf{I}_3 & \mathbf{0}_{3N \times N} \\ \mathbf{0}_{N \times 3N} & \mathbf{0}_N \end{bmatrix} \in \mathbb{R}^{4N}$, $\hat{\mathbf{L}} = \begin{bmatrix} \mathbf{L} \otimes \mathbf{I}_3 & \mathbf{0}_{3N \times N} \\ \mathbf{0}_{N \times 3N} & \mathbf{0}_N \end{bmatrix} \in \mathbb{R}^{4N}$, $\boldsymbol{\Theta}_f = \begin{bmatrix} (\mathbf{D} \mathbf{W}_f \otimes \mathbf{I}_3) \mathbf{d} \\ \mathbf{0}_{N \times 1} \end{bmatrix} \in \mathbb{R}^{4N \times 1}$, $\boldsymbol{\Theta} = \begin{bmatrix} (\mathbf{D} \mathbf{W} \otimes \mathbf{I}_3) \mathbf{d} \\ \mathbf{0}_{N \times 1} \end{bmatrix} \in \mathbb{R}^{4N \times 1}$, $\boldsymbol{\Upsilon}_f = \mathbf{d}^\top (\mathbf{W}_f \otimes \mathbf{I}_3) \mathbf{d} \in \mathbb{R}$, $\boldsymbol{\Upsilon} = \mathbf{d}^\top (\mathbf{W} \otimes \mathbf{I}_3) \mathbf{d} \in \mathbb{R}$, $\mathbf{L}_f = \mathbf{D} \mathbf{W}_f \mathbf{D}^\top \in \mathbb{R}^N$, $\mathbf{W}_f = \text{diag}(\dots, \omega_{ij}, \dots) \forall (i, j) \in \mathcal{E} \in \mathbb{R}^{|\mathcal{E}|}$, and $\mathbf{d} = [\dots, \mathbf{d}_{ij}^\top, \dots]^\top \in \mathbb{R}^{3|\mathcal{E}|}$. The matrices \mathbf{Q}_f and \mathbf{Q} are symmetric and PSD (note that $\mathbf{r}^\top(t_f) \mathbf{Q}_f \mathbf{r}(t_f) \geq 0$, $\mathbf{r}^\top(t) \mathbf{Q} \mathbf{r}(t) \geq 0$).

The convexity of the objective functional (7) and dynamics (6) makes Pontryagin's principle both necessary and sufficient for optimality. Applying these conditions, the optimal formation trajectory planning signal for any initial state of the UAV team is presented as follows.

Theorem 1. *Consider the multi-UAV formation control problem in flat coordinates defined by (6) and (7). The optimal formation trajectory for any initial state \mathbf{r}_0 is given by*

$$\mathbf{r}(t) = \mathbf{H}(t_f - t) \mathbf{H}^{-1}(t_f) \mathbf{r}_0, \quad (8)$$

where

$$\mathbf{H}(t) = [\mathbf{I} \quad \mathbf{0}] \exp(-t\mathbf{M}) \begin{bmatrix} \mathbf{I} \\ \mathbf{Q}_f \end{bmatrix}, \quad (9)$$

$$\mathbf{M} = \begin{bmatrix} \mathbf{A} & -\mathbf{B}\mathbf{R}^{-1}\mathbf{B}^\top \\ -\mathbf{Q} & -\mathbf{A}^\top \end{bmatrix}. \quad (10)$$

Proof. See Appendix A. □

4.2 Formation trajectory tracking

In the control scheme depicted in Fig. 3, the formation trajectory planning signal described in (8) is followed by the formation trajectory tracker. Meanwhile, the tracker should ensure that each UAV avoids collisions with its neighboring UAVs along its specified trajectory when $\Gamma(\mathbf{p})$ becomes non-empty.

4.2.1 safety region control strategy

When $\Psi(\mathbf{p}) \neq \emptyset$, the UAVs are within the safety region, and thus the inter-UAV collision avoidance constraint is inactive. The control strategy for the UAVs to follow the formation trajectory planning signal within the safety region is derived as follows.

Using the finite-time linear quadratic regulator paradigm, formation trajectory tracking within the safety region is recast as the following optimal control problem

$$\begin{aligned} & \min_{\mathbf{u}_z} (\mathbf{z}(t_f) - \mathbf{r}(t_f))^\top \mathbf{K}_f (\mathbf{z}(t_f) - \mathbf{r}(t_f)) + \\ & \int_0^{t_f} \left\{ (\mathbf{z}(t) - \mathbf{r}(t))^\top \mathbf{K} (\mathbf{z}(t) - \mathbf{r}(t)) + \mathbf{u}_z^\top(t) \mathbf{R}_z \mathbf{u}_z(t) \right\} dt, \end{aligned} \quad (11)$$

subject to

$$\dot{\mathbf{z}}(t) = \mathbf{A}\mathbf{z}(t) + \mathbf{B}\mathbf{u}_z(t), \quad \mathbf{z}(0) = \mathbf{r}_0, \quad (12)$$

where $\mathbf{K}_f = \text{diag}(\mathbf{K}_{0f}, 0)$, $\mathbf{K}_{0f} = \mathbf{I}_3 \otimes \text{diag}(\delta_1, \dots, \delta_N) \otimes \mathbf{I}_4$, $\mathbf{K} = \text{diag}(\mathbf{K}_0, 0)$, $\mathbf{K}_0 = \mathbf{I}_3 \otimes \text{diag}(\zeta_1, \dots, \zeta_N) \otimes \mathbf{I}_4$, $\mathbf{R}_z = \text{diag}(\eta_1, \dots, \eta_N) \otimes \mathbf{I}_4$, $\delta_i > 0$, $\zeta_i > 0$, and $\eta_i > 0$.

The optimal feedback control for (11) and (12) is given by

$$\mathbf{u}_z(t) = -\mathbf{R}_z^{-1} \mathbf{B}^\top \mathbf{P}(t) (\mathbf{z}(t) - \mathbf{r}(t)), \quad (13)$$

where $\mathbf{P}(t)$ is the solution to the Riccati differential equation

$$\begin{aligned} & \dot{\mathbf{P}}(t) + \mathbf{P}(t)\mathbf{A} - \mathbf{P}(t)\mathbf{B}\mathbf{R}_z^{-1}\mathbf{B}^\top\mathbf{P}(t) + \mathbf{K} + \mathbf{A}^\top\mathbf{P}(t) = \mathbf{0}, \\ & \mathbf{P}(t_f) = \mathbf{K}_f. \end{aligned} \quad (14)$$

The pair (\mathbf{A}, \mathbf{B}) is controllable, $\mathbf{R}_z \succ 0$, and $\mathbf{K} \succ 0$, thus, there exists a unique solution $\mathbf{P}(t) = \mathbf{P}^\top(t) \succeq 0$ to (14).

The optimal state feedback is given by

$$\dot{\mathbf{z}}(t) = (\mathbf{A} - \mathbf{B}\mathbf{R}_z^{-1}\mathbf{B}^\top\mathbf{P}(t)) (\mathbf{z}(t) - \mathbf{r}(t)). \quad (15)$$

And the minimal cost attained at any $t \in [0, t_f]$ and state $\mathbf{z}(t)$ is yielded by the value function

$$n(\mathbf{z}) = (\mathbf{z}(t) - \mathbf{r}(t))^\top \mathbf{P}(t)(\mathbf{z}(t) - \mathbf{r}(t)). \quad (16)$$

The Hamilton–Jacobi–Bellman (HJB) equation is given by

$$\frac{dn}{dt} + \min_{\mathbf{u}_z} \{ (\mathbf{z}(t) - \mathbf{r}(t))^\top \mathbf{K}(\mathbf{z}(t) - \mathbf{r}(t)) + \mathbf{u}_z^\top(t) \mathbf{R}_z \mathbf{u}_z(t) + \frac{\partial n}{\partial \mathbf{z}} (\mathbf{A}\mathbf{z}(t) + \mathbf{B}\mathbf{u}_z(t)) \} = 0. \quad (17)$$

And the optimal input (13) equivalently is derived from the HJB equation (17) as

$$\mathbf{u}_z(t) = -\mathbf{R}_z^{-1} \mathbf{B}^\top \frac{\partial n}{\partial \mathbf{z}}.$$

4.2.2 collision avoidance control strategy

When $\Gamma(\mathbf{p}) \neq \emptyset$, the formation trajectory tracker applies the collision avoidance control strategy derived below for the collision reaction region.

First, we define a collision penalty function [26, 8] as

$$v_{ij} = \left(\min \left\{ 0, \frac{\|\mathbf{p}_j(t) - \mathbf{p}_i(t)\|^2 - (R_i + R_j)^2}{\|\mathbf{p}_j(t) - \mathbf{p}_i(t)\|^2 - (r_i + r_j)^2} \right\} \right)^2 = \left(\min \left\{ 0, \frac{\|\mathbf{e}_{ij}^\top \mathbf{z}(t)\|^2 - (R_i + R_j)^2}{\|\mathbf{e}_{ij}^\top \mathbf{z}(t)\|^2 - (r_i + r_j)^2} \right\} \right)^2, \quad (18)$$

for all $(i, j) \in \mathcal{E}_c$ where $\mathbf{e}_{ij} = [-\mathbf{D}_{ij} \otimes \mathbf{I}_3, \mathbf{0}] \in \mathbb{R}^{(12N+1) \times 3}$ and \mathbf{D}_{ij} is the column of \mathbf{D} corresponding to the edge (i, j) . Note that v_{ij} is nonzero only within the collision reaction region and is either zero or undefined outside of this region.

The partial derivative of v_{ij} with respect to \mathbf{z}_i is given by

$$\frac{\partial v_{ij}}{\partial \mathbf{z}_i} = \begin{cases} \mathbf{0}, & \text{if } \Psi(\mathbf{p}) \neq \emptyset \\ \mathbf{z}^\top(t) \mathbf{e}_{ij} \phi_{ij}, & \text{if } \Gamma(\mathbf{p}) \neq \emptyset \\ \mathbf{0}, & \text{if } \Lambda(\mathbf{p}) \neq \emptyset \\ \text{not defined,} & \text{if } \Phi(\mathbf{p}) \neq \emptyset \end{cases}$$

where

$$\phi_{ij} = 4((R_i + R_j)^2 - (r_i + r_j)^2) \frac{\|\mathbf{e}_{ij}^\top \mathbf{z}(t)\|^2 - (R_i + R_j)^2}{(\|\mathbf{e}_{ij}^\top \mathbf{z}(t)\|^2 - (r_i + r_j)^2)^3}.$$

Moreover, the time derivative of v_{ij} at the collision reaction region (i.e., at $\Gamma(\mathbf{p}) \neq \emptyset$) is

$$\frac{dv_{ij}}{dt} = \frac{\partial v_{ij}}{\partial \mathbf{z}_i} \mathbf{e}_{ij}^\top \dot{\mathbf{z}}(t). \quad (19)$$

Let $V_i = \sum_{j \in \mathcal{N}_i} v_{ij}$ where $\frac{\partial V_i}{\partial \mathbf{z}_i} = \sum_{j \in \mathcal{N}_i} \mathbf{z}^\top(t) \mathbf{e}_{ij} \phi_{1j}$ for all $i \in \mathcal{V}$. Define $\frac{\partial V}{\partial \mathbf{z}} = [\mathbf{0}_{8N}, \frac{\partial V_1}{\partial \mathbf{z}_1}, \dots, \frac{\partial V_N}{\partial \mathbf{z}_N}, \mathbf{0}_{N+1}] \in \mathbb{R}^{12N+1}$.

Now, redefine the HJB in (17) as

$$\begin{aligned} & \left(\frac{dn}{dt} + \frac{dV}{dt} \right) + \min_{\mathbf{u}_z} \{ (\mathbf{z}(t) - \mathbf{r}(t))^\top \mathbf{K}(\mathbf{z}(t) - \mathbf{r}(t)) + \mathbf{u}_z^\top(t) \mathbf{R}_z \mathbf{u}_z(t) + \\ & \left(\frac{\partial n}{\partial \mathbf{z}} + \frac{\partial V}{\partial \mathbf{z}} \right) (\mathbf{A}\mathbf{z}(t) + \mathbf{B}\mathbf{u}_z(t)) \} = 0, \end{aligned} \quad (20)$$

Note that the HJB in (20) is constructed for the tracking optimal control problem with the performance index (11), augmented with a penalty function to indirectly designate the collision region instead of the inequality constraint to ensure safety [17].

The collision avoidance control strategy is obtained by minimizing (20) which yields the feedback control law

$$\mathbf{u}_z(t) = -\mathbf{R}_z^{-1}\mathbf{B}^\top\left(\mathbf{P}(t)\mathbf{z}(t) + \frac{\partial V^\top}{\partial \mathbf{z}}\right). \quad (21)$$

The state feedback is given by

$$\dot{\mathbf{z}}(t) = (\mathbf{A} - \mathbf{B}\mathbf{R}_z^{-1}\mathbf{B}^\top\mathbf{P}(t))\mathbf{z}(t) - \mathbf{B}\mathbf{R}_z^{-1}\mathbf{B}^\top\frac{\partial V^\top}{\partial \mathbf{z}}. \quad (22)$$

The collision avoidance control law outside the collision reaction region (i.e., within the safety region) coincides with the optimal control law in the safety region.

To show that (21) constitutes a collision-free control strategy, we prove that (20) is non-increasing in $\Gamma(\mathbf{p})$ [26].

Let $\hat{V} = \sum_{i=1}^N V_i$.

Lemma 1. *If the initial conditions of the UAVs satisfy*

$$\|\mathbf{p}_i(0) - \mathbf{p}_j(0)\| \geq r_i + r_j + \epsilon, \quad (23)$$

for all $i, j \in \mathcal{V}$, $i \neq j$, and some $\epsilon > 0$, then the UAVs can achieve $\frac{d\hat{V}}{dt} \geq 0$ using bounded control effort, thereby avoiding collisions.

Proof. Let $\frac{d\hat{V}}{dt} < 0$, since any other condition trivially satisfies Lemma 1. By the fundamental theorem of calculus,

$$\hat{V}(t) = \hat{V}(0) + \int_0^t \frac{d\hat{V}}{d\tau} d\tau. \quad (24)$$

The control input \mathbf{u}_z explicitly appears in $\frac{d^{n+1}\hat{V}}{dt^{n+1}}$ (i.e., $n = 2$ here). We can obtain $\hat{V}(t)$ and $\frac{d\hat{V}}{dt}$ as a function of \mathbf{u}_z ,

$$\hat{V}(t) = \hat{V}(0) + \sum_{i=1}^n \frac{d^i \hat{V}}{dt^i} \Big|_{t=0} \frac{t^i}{i!} + \underbrace{\int_0^t \cdots \int_0^t}_{n+1} \frac{d^{n+1} \hat{V}}{d\tau^{n+1}} \underbrace{d\tau \cdots d\tau}_{n+1}, \quad (25)$$

$$\frac{d\hat{V}}{dt} = \sum_{i=1}^n \frac{d^i \hat{V}}{dt^i} \Big|_{t=0} \frac{t^{i-1}}{(i-1)!} + \underbrace{\int_0^t \cdots \int_0^t}_n \frac{d^{n+1} \hat{V}}{d\tau^{n+1}} \underbrace{d\tau \cdots d\tau}_n, \quad (26)$$

where $\frac{d^n \hat{V}}{dt^n} \Big|_{t=0}$ is the initial condition of the n^{th} derivative of $\hat{V}(t)$.

To guarantee collision avoidance while $\frac{d\hat{V}}{dt} \rightarrow 0$ at time t , we require

$$\hat{V}(t) \leq \hat{V}(0) + \delta, \quad (27)$$

$$\frac{d\hat{V}}{dt} \leq 0, \quad (28)$$

where $\delta > 0$ and (27) implies collision avoidance, as $\frac{d\hat{V}}{dt} > 0$ implies that $\hat{V}(t) = \max_{\tau \in [0, t]} \hat{V}(\tau)$. Substituting (25) and (26) into (27) and (28), respectively, and rearranging their terms yield

$$\underbrace{\int_0^t \cdots \int_0^t}_{n+1} \frac{d^{n+1}\hat{V}}{d\tau^{n+1}} \underbrace{d\tau \cdots d\tau}_{n+1} \leq -\left(\delta + \sum_{i=1}^n \frac{d^i \hat{V}}{dt^i} \Big|_{t=0} \frac{t^n}{n!}\right), \quad (29)$$

$$\underbrace{\int_0^t \cdots \int_0^t}_{n} \frac{d^{n+1}\hat{V}}{d\tau^{n+1}} \underbrace{d\tau \cdots d\tau}_n \leq -\sum_{i=1}^n \frac{d^i \hat{V}}{dt^i} \Big|_{t=0} \frac{t^{n-1}}{(n-1)!}. \quad (30)$$

Both (29) and (30) are finite lower bounds on the function $\frac{d^{n+1}\hat{V}}{dt^{n+1}}$. Therefore, we can always construct a finite function $\frac{d^{n+1}\hat{V}}{dt^{n+1}}$ to satisfy (29) and (30) for an arbitrarily small $t > 0$. This implies that (27) and (28) are satisfied for any $\delta > 0$. Finally, by continuity in $\frac{d\hat{V}}{dt}$, we can select δ sufficiently small to ensure (27) and (28) for any $\epsilon > 0$. This concludes the proof. \square

Theorem 2. *Given the conditions of Lemma 1, any trajectory that results in a collision is sub-optimal.*

Proof. We use a proof by contradiction. Assume that a trajectory where two UAVs collide is optimal, resulting in a cost of $J^* = \infty$ by definition. By Lemma 1, there exists a bounded control input \mathbf{u}_z^\dagger such that $\frac{d\hat{V}}{dt} \Big|_{t=t^\dagger} = 0$ in some finite time $t^\dagger < t_f$ without collisions. The corresponding cost is

$$J^\dagger = \int_0^{t^\dagger} \left\{ (\mathbf{z}(t) - \mathbf{r}(t))^\top \mathbf{K}(\mathbf{z}(t) - \mathbf{r}(t)) + (\mathbf{u}_z^\dagger(t))^\top \mathbf{R}_z \mathbf{u}_z^\dagger(t) + \frac{d\hat{V}}{dt} \right\} dt \\ + \int_{t^\dagger}^{t_f} \left\{ (\mathbf{z}(t) - \mathbf{r}(t))^\top \mathbf{K}(\mathbf{z}(t) - \mathbf{r}(t)) + (\mathbf{u}_z^\dagger(t))^\top \mathbf{R}_z \mathbf{u}_z^\dagger(t) \right\} dt, \quad (31)$$

where V remains stationary for $t \geq t^\dagger$. Every term in (31) is finite. Therefore, $J^\dagger < J^*$ and J^* is not optimal. This contradiction implies that our original assumption is incorrect, proving Theorem 2. \square

5 Directionally Aware Collision Avoidance

In this section, we introduce two collision avoidance strategies that incorporate directional awareness by integrating the UAVs' velocities into the collision penalty function in Subsection 4.2.2. Recognizing that combining these strategies enhances the effectiveness of collision avoidance, we unify them into a single approach to provide UAVs with a more robust, directionally aware collision avoidance capability.

5.1 Forward-path aware collision avoidance

To derive a collision avoidance control strategy that is directionally aware, we adjust the penalty function to prioritize avoiding collisions in the forward path of each UAV. We incorporate a forward-path aware weighting factor α_{ij} into the collision penalty function (18) as

$$v_{ij}^F = \alpha_{ij} v_{ij},$$

where

$$\alpha_{ij} = \begin{cases} \max\{0, \cos(\eta_{ij})\}, & \text{if } \|\mathbf{v}_i(t)\| \neq 0, \\ 0, & \text{if } \|\mathbf{v}_i(t)\| = 0, \end{cases} \quad (32)$$

with

$$\cos(\eta_{ij}) = \frac{(\mathbf{p}_j(t) - \mathbf{p}_i(t))^\top \mathbf{v}_i(t)}{\|\mathbf{p}_j(t) - \mathbf{p}_i(t)\| \|\mathbf{v}_i(t)\|}.$$

The forward-path aware penalty function v_{ij}^F accounts for whether UAV j lies within the forward path of UAV i , and it is zero otherwise. Specifically, when UAV j is in the forward path, the directionally aware weighting factor is given by the cosine of the angle between the relative position vector and the velocity vector, as depicted in Fig. 4. The cosine is obtained using the dot product as shown in (32). If UAV j is positioned behind UAV i , the weighting factor is zero.

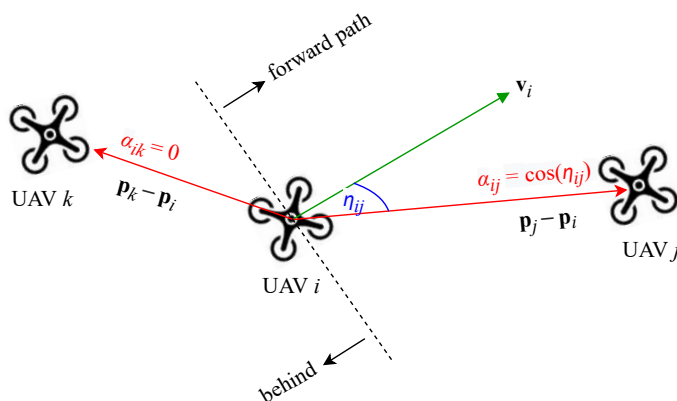


Figure 4: The forward-path aware collision avoidance prioritizes avoiding collisions in the forward path. The velocity vector \mathbf{v}_i indicates the forward motion path of UAV i . Within the collision reaction region, when UAV j is located in the forward path of UAV i , the directionally aware weighting factor α_{ij} for UAV i with respect to UAV j is defined as the cosine of the angle between the UAV i 's velocity vector \mathbf{v}_i and their relative distance vector $\mathbf{p}_j - \mathbf{p}_i$. The value of α_{ij} decreases as the UAV j moves further to the sides. By definition, α_{ik} is zero when UAV k is located behind UAV i .

5.2 Approach-aware collision avoidance

In approach-aware collision avoidance, the collision penalty function is adjusted to prevent a collision when two UAVs are on an approach trajectory. This approach leverages the relative velocities to assess whether the UAVs are approaching each other. The approach-aware weighting factor β_{ij} is incorporated into (18) as

$$v_{ij}^A = \beta_{ij} v_{ij},$$

where

$$\beta_{ij} = \begin{cases} \max\{0, -\cos(\zeta_{ij})\}, & \text{if } \|\mathbf{v}_j(t) - \mathbf{v}_i(t)\| \neq 0, \\ 0, & \text{if } \|\mathbf{v}_j(t) - \mathbf{v}_i(t)\| = 0, \end{cases}$$

with

$$\cos(\zeta_{ij}) = \frac{(\mathbf{p}_j(t) - \mathbf{p}_i(t))^\top (\mathbf{v}_j(t) - \mathbf{v}_i(t))}{\|\mathbf{p}_j(t) - \mathbf{p}_i(t)\| \|\mathbf{v}_j(t) - \mathbf{v}_i(t)\|}.$$

Here, $\cos(\zeta_{ij})$ captures the alignment between the relative position $\mathbf{p}_j(t) - \mathbf{p}_i(t)$ and velocity $\mathbf{v}_j(t) - \mathbf{v}_i(t)$. When $\cos(\zeta_{ij}) < 0$, the UAVs are approaching, posing a collision risk. If their velocities are identical, i.e., $\|\mathbf{v}_j(t) - \mathbf{v}_i(t)\| = 0$, they remain at a constant separation. A higher β_{ij} (near 1) indicates a direct, high-speed approach, while a lower β_{ij} (closer to 0) suggests an oblique approach with reduced collision risk. When $\beta_{ij} = 0$, the UAVs are either parallel, diverging, or stationary relative to each other.

5.3 Directionally aware unified collision avoidance

We combine the collision avoidance strategies from Subsections 5.1 and 5.2 into a unified approach that accounts for both UAV j being within UAV i 's forward path and the relative approach. This is achieved by defining the weighting factor ξ_{ij} as:

$$\xi_{ij} = \alpha_{ij} \beta_{ij},$$

or

$$\xi_{ij} = \begin{cases} \max\{0, \cos(\eta_{ij})\} \max\{0, -\cos(\zeta_{ij})\}, & \text{if } \|\mathbf{v}_i(t)\| \neq 0 \text{ and } \|\mathbf{v}_j(t) - \mathbf{v}_i(t)\| \neq 0, \\ 0, & \text{otherwise.} \end{cases}$$

Here, α_{ij} ensures that UAV j is in the forward path of UAV i . If UAV j is outside the forward path, $\alpha_{ij} = 0$, making $\xi_{ij} = 0$. β_{ij} ensures that UAV j is approaching UAV i . If UAV j is moving away or stationary relative to UAV i , $\beta_{ij} = 0$, making $\xi_{ij} = 0$. Thus, ξ_{ij} is nonzero only when UAV j lies in the forward path of UAV i ($\alpha_{ij} > 0$) and UAV j is approaching UAV i ($\beta_{ij} > 0$) and is zero if either condition is not met.

To demonstrate the improved effectiveness of the unified collision avoidance approach, we analyze two scenarios with two UAVs having evolving positions and velocities. In the first scenario, $\mathbf{p}_1(0) = [1, 1]^\top$ and $\mathbf{p}_2(0) = [7, 0]^\top$; in the second, $\mathbf{p}_2(0)$ is changed to $[7, 3]^\top$. Both scenarios feature constant velocities $\mathbf{v}_1(0) = [2, 1]^\top$ and $\mathbf{v}_2(0) = [-2, 1]^\top$. The evolution of relative vectors, α_{12} , β_{12} , and ξ_{12} at some time steps are shown in Fig. 5. Figs. 5a–5d represent the first scenario, while Figs. 5e–5h depict the second. Figs. 5d and 5h compare α_{12} and β_{12} over 20 time steps. It is evident that ξ_{12} consistently captures collision risks more effectively and shows to be more reliable overall.

We then incorporate the directionally aware penalty function v_{ij}^U defined as

$$v_{ij}^U = \xi_{ij} v_{ij},$$

into the HJB equation, replacing v_{ij} with v_{ij}^U in the minimization to account for the new penalty function. In the feedback control law $\mathbf{u}_z(t)$ in (21) now $\frac{\partial V}{\partial \mathbf{z}}$ accounts for the directionally aware collision avoidance strategy. This approach provides a collision avoidance control that emphasizes avoiding collisions in the forward path as well as along an approach trajectory, promoting adaptive behavior, and enhancing collision-free formation tracking efficiency.

6 Simulation Results

In this section, we consider a four-UAV ($N = 4$) (re)formation problem to demonstrate the efficacy of the presented control scheme outlined in Fig. 3. In the initial configuration, the UAVs are

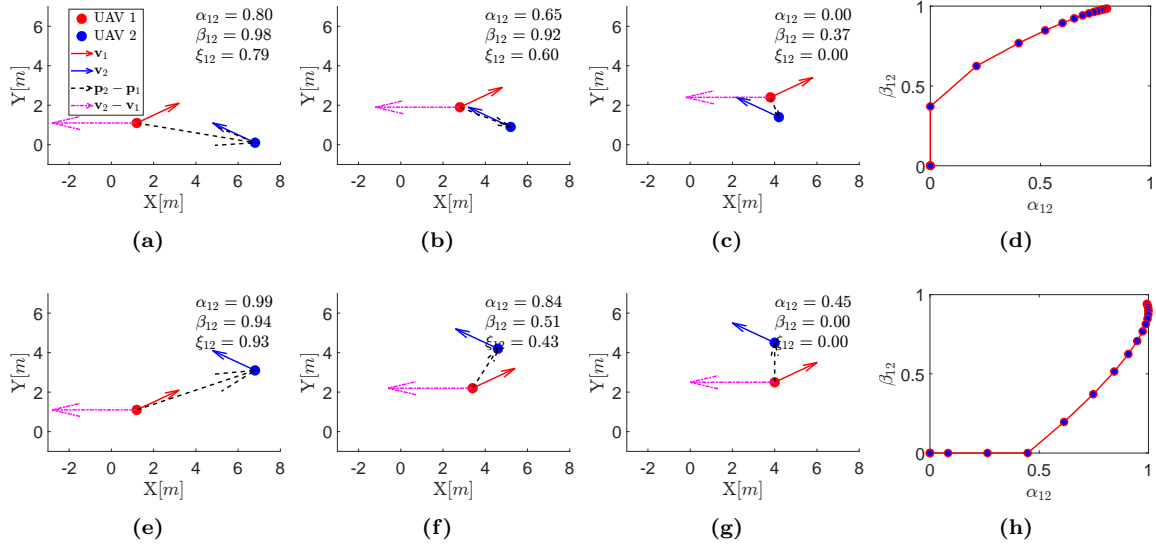


Figure 5: Evolution of relative vectors, α_{12} , β_{12} , and ξ_{12} for two UAVs in two scenarios. Scenario 1 is depicted in subfigures (a) to (d), and Scenario 2 in subfigures (e) to (h).

positioned in a square formation in the $x - y$ plane from the top, as illustrated in Fig. 6a. The formation shape is determined by the offset vectors $\mathbf{d}_{12} = [-4m, -4m, 0m]^\top$ and $\mathbf{d}_{13} = \mathbf{d}_{24} = [4m, -4m, 0m]^\top$, which characterize a diamond alignment in the $x - y$ plane, as depicted in Fig. 6b.

The initial states of the UAVs in the flat coordinates are $\mathbf{p}_1(0) = [0m, 0m, 5m]^\top$, $\mathbf{p}_2(0) = [5m, 0m, 0m]^\top$, $\mathbf{p}_3(0) = [0m, 5m, 0m]^\top$, $\mathbf{p}_4(0) = [5m, 5m, 0m]^\top$, $\dot{\mathbf{p}}_i(0) = [0m/s, 0m/s, 0m/s]^\top$, $\ddot{\mathbf{p}}_i(0) = [0m/s^2, 0m/s^2, 0m/s^2]^\top$, and $\psi_i(0) = 0rad$, $\dot{\psi}_i(0) = 0rad/s$, $\ddot{\psi}_i(0) = 0rad/s^2$ for $i \in \{1, 2, 3, 4\}$. The weighting parameters of the performance index (7) are as $\mu_{12} = 0.9$, $\mu_{13} = 0.7$, $\mu_{14} = 0.5$, $\mu_{23} = 0.6$, $\mu_{24} = 0.8$, $\mu_{34} = 0.4$, $\omega_{ij} = 1$ for all $(i, j) \in \mathcal{E}_f$, and $\gamma_i = 1$ for all $i \in \{1, 2, 3, 4\}$. The horizon length is $t_f = 10s$. For each UAV, its mass, distance from the rotor to the center of mass, gravity acceleration, and moment of inertia are respectively set as $m = 1.0kg$, $0.2m$, $g = 9.81m/s^2$, and $\mathcal{I}_{xx} = \mathcal{I}_{yy} = \mathcal{I}_{zz} = 0.016kg \cdot m^2$.

The optimal formation trajectories of the UAV team, generated from Theorem 1, and the corresponding time histories are shown in Figs. 7–8, respectively. In the absence of inter-UAV collision avoidance, these trajectories highlight the optimality of the UAV team control strategies in achieving the prescribed diamond formation within the designated finite time interval.

The formation trajectory tracking involves tracking the optimal formation trajectory planning signal while considering inter-UAV collisions, as outlined in Fig. 3. The avoidance region radius for all UAVs is defined as the same value $r_i = 1.5m$ for all $i = 1, \dots, 4$. This implies that a collision occurs for every UAV pair (i, j) if they approach each other closer than $3m$. We choose the radius of the collision reaction region $R_i = 2r_i$ for all $i = 1, \dots, 4$. The parameters of the tracking performance index (11) are set as $\zeta_{ij} = 10\mu_{ij}$, $\delta_{ij} = 10\omega_{ij}$, and $\eta_i = \gamma_i$ for all $i, j \in \{1, 2, 3, 4\}$ and (i, j) in the communication graph. Utilizing the collision penalty function from Subsection 4.2.2, the formation tracking trajectories and their corresponding time histories are shown in Figs. 9–10, respectively. It is apparent from both figures that the UAV team tracks the optimal trajectories and successfully achieves the desired formation at the terminal time. The relative distances between

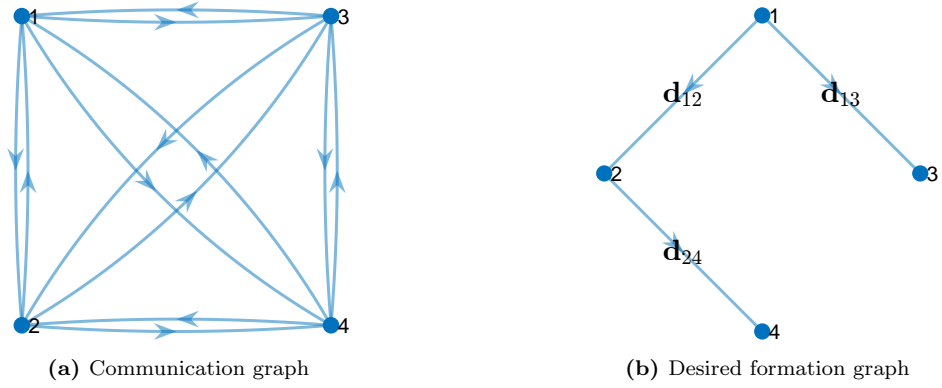


Figure 6: The communication graph $\mathcal{G}_c(\mathcal{V}, \mathcal{E}_c)$ and the desired formation graph $\mathcal{G}_f(\mathcal{V}, \mathcal{E}_f)$ for a team of four UAVs. The graphs illustrate the spatial arrangement of the UAVs in the x - y plane, corresponding to their initial and desired formations, respectively.

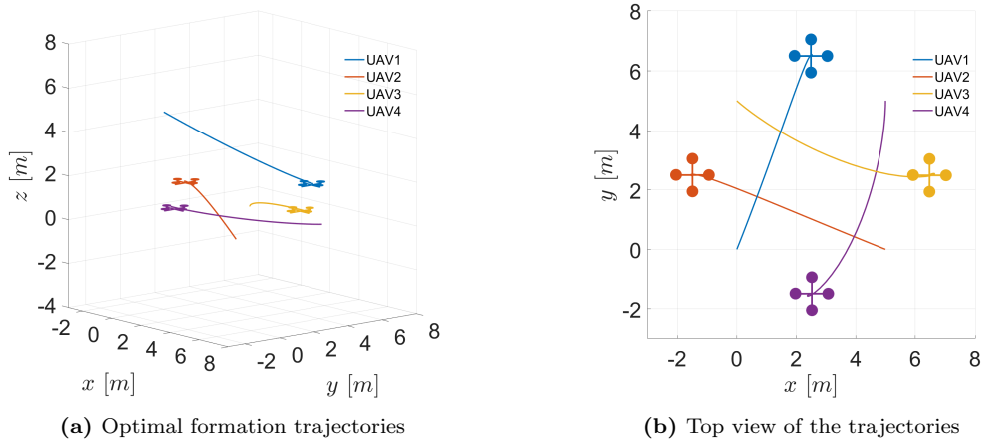


Figure 7: Optimal formation trajectories of UAVs. Initially, the UAVs are placed such that from the top, they are seen in a square formation and then transition into a diamond formation in the x - y plane.

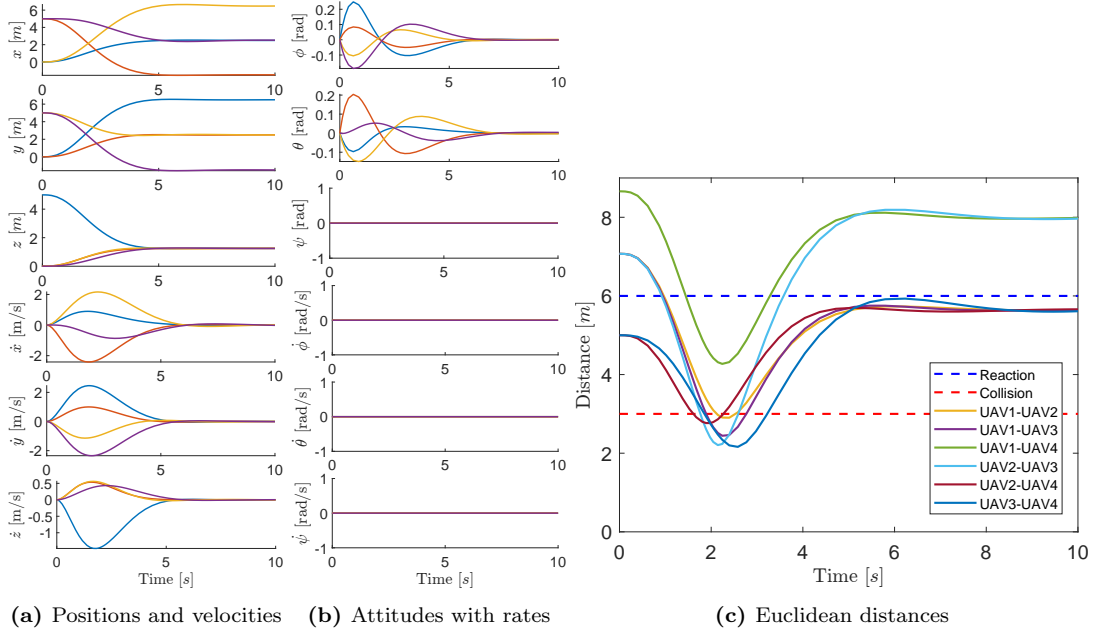


Figure 8: Time histories of positions, velocities, and Euclidean distances for all UAV pairs $(i, j) \in \mathcal{E}_f$. The blue dashed line represents the distance before entering the collision reaction region (i.e., $R_i + R_j$), and the red dashed line represents the distance before entering the collision region (i.e., $r_i + r_j$).

any UAV pair never decrease below $r_i + r_j$, even though some UAV pairs initially have a relative distance between $r_i + r_j$ and $R_i + R_j$. Despite the collision avoidance control strategy being applied from the outset, it separates the UAV pairs before they reach the collision region.

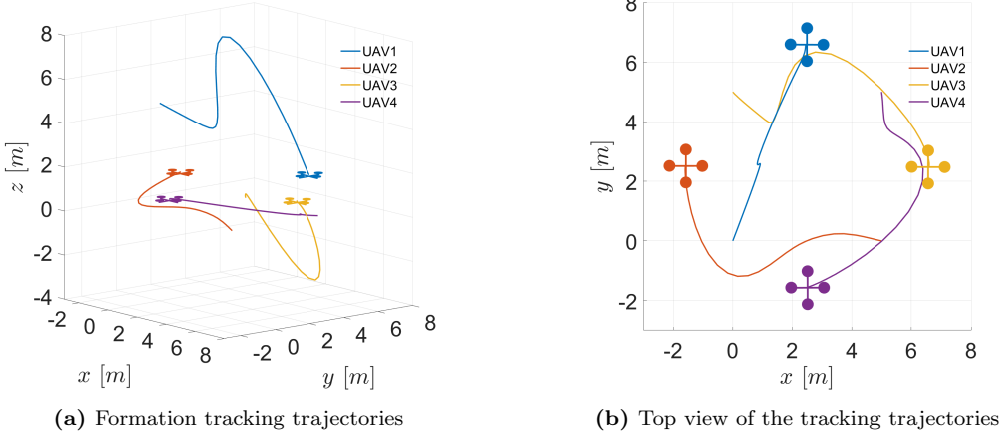


Figure 9: Formation trajectory tracking, which involves following the optimal formation trajectory while accounting for inter-UAV collisions.

The formation trajectories and their corresponding time histories using the directionally aware collision avoidance tracking strategy are shown in Fig. 11–12, respectively. Unlike the non-directionally aware approach in Figs. 9-10, where UAVs significantly deviate from their optimal planned paths to avoid collisions, the directionally aware collision avoidance strategy permits minimal deviations from the optimal trajectory. The results highlight the effectiveness of the proposed formation trajectory planning and tracking, demonstrating successful collision-free multi-UAV formation control. Notably, UAVs employing the directionally aware collision avoidance strategy require minimal deviation from their optimal paths to ensure collision avoidance. Thus, the directionally aware collision avoidance approach proves more efficient by adaptively prioritizing collision avoidance in both the forward path and the relative approach for each UAV.

7 Conclusion

In this paper, we present a collision-free finite-time formation control scheme for multiple UAVs based on the differential flatness property of UAV dynamics. Unlike traditional approaches that rely on a leader, predefined tracking signals, or waypoints, our method leverages the initial states of the UAVs to plan optimal formation trajectories. Moreover, the proposed approach introduces a directionally aware collision avoidance strategy that prioritizes collision avoidance both in the forward path and the relative approach for each UAV, promoting adaptive behavior and enhancing efficiency. By addressing a finite-time optimal control problem, we derived a trajectory that optimizes a collective performance index, ensuring efficient formation and movement. Additionally, we tackled the collision-constrained regulating problem to maintain collision-free tracking of the formation trajectory. We trade optimality for safety guarantees in the tracking controller when necessary. The simulation results validated the efficacy of our control scheme.

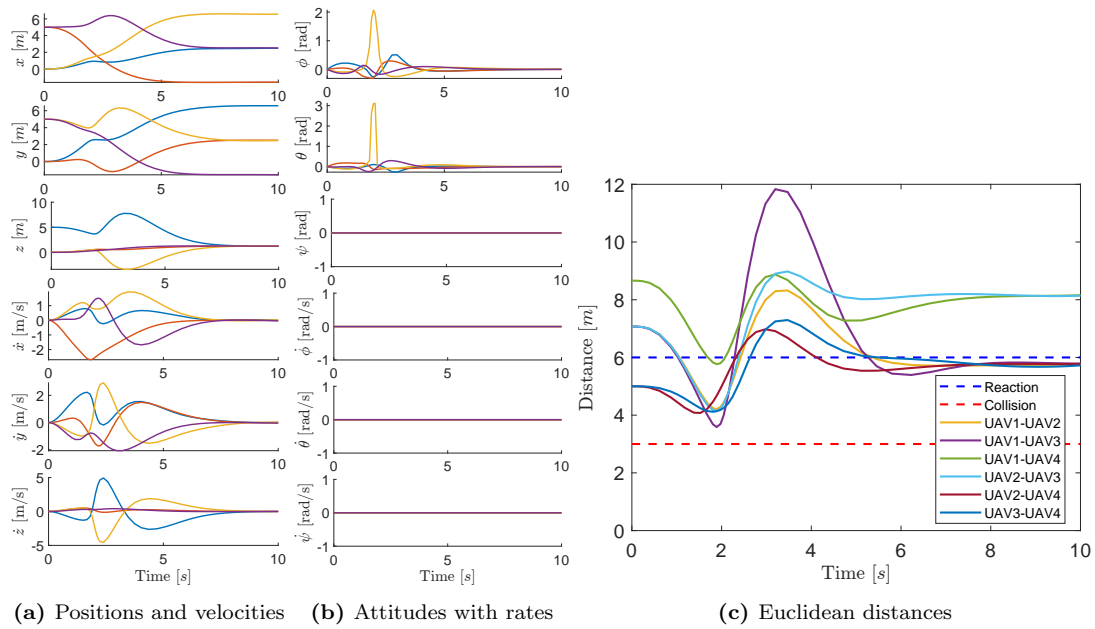


Figure 10: Time histories of positions, velocities, and Euclidean distances for formation tracking trajectories.

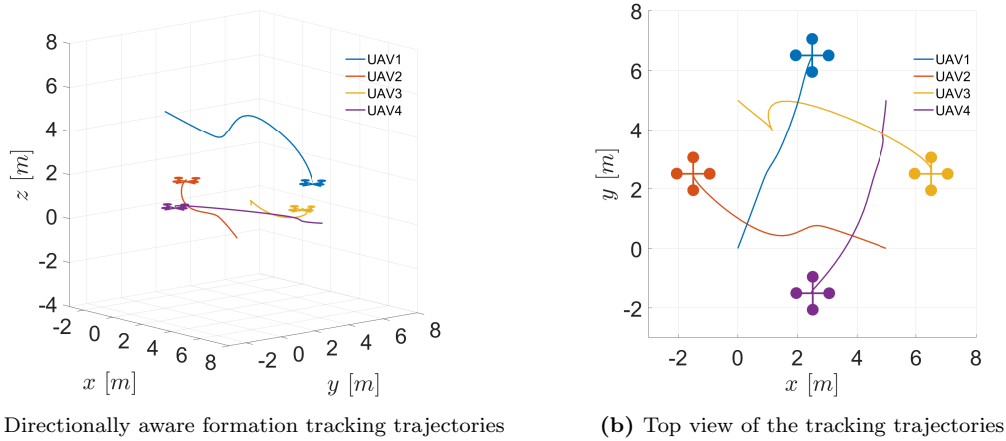


Figure 11: Formation trajectory tracking utilizing the directionally aware collision avoidance strategy.

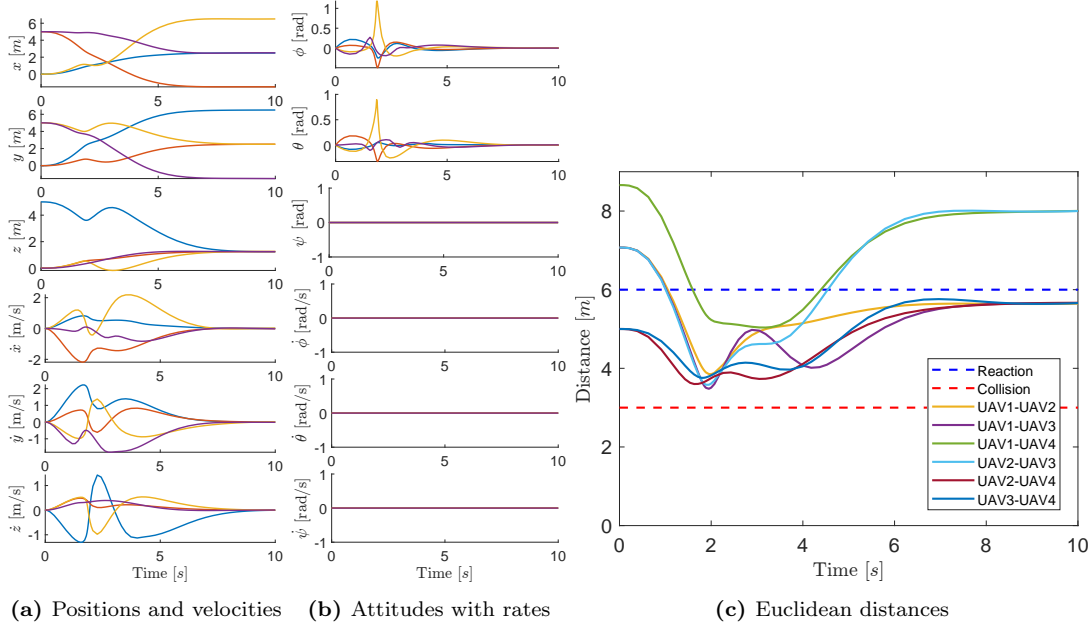


Figure 12: Time histories of positions, velocities, and Euclidean distances for formation tracking trajectories utilizing the directionally aware collision avoidance strategy.

The assumption of a complete communication graph to ensure global collision avoidance awareness may result in scalability challenges for larger UAV teams. Future work could address this limitation by developing distributed control strategies that enable real-time, directionally aware, collision-free trajectory planning and tracking for physical UAVs using onboard sensors such as UVDAR [27].

Acknowledgments

This work was partially funded by the Czech Science Foundation (GAČR) under research project no. 23 – 07517S and the European Union under the project Robotics and Advanced Industrial Production (reg. no. CZ.02.01.01/00/22_008/0004590), Czech Technical University in Prague (CTU) within the CTU Global Postdoc Fellowship program, and CTU grant no. SGS23/177/OHK3/3T/13.

A proof of theorem 1

Proof. Define the Hamiltonian

$$H = \mathbf{r}^\top(t)\mathbf{Q}\mathbf{r}(t) + \mathbf{u}_r^\top(t)\mathbf{R}\mathbf{u}_r(t) + \boldsymbol{\psi}^\top(t)(\mathbf{A}\mathbf{r}(t) + \mathbf{B}\mathbf{u}_r(t)), \quad (33)$$

where $\boldsymbol{\psi}(t)$ is co-state. According to Pontryagin's principle, the necessary conditions for optimality are $\frac{\partial H}{\partial \mathbf{u}_r} = 0$ and $\dot{\boldsymbol{\psi}}(t) = -\frac{\partial H}{\partial \mathbf{r}}$. Applying the necessary conditions yields

$$\mathbf{u}_r(t) = -\mathbf{R}^{-1}\mathbf{B}^\top \boldsymbol{\psi}(t), \quad (34)$$

$$\dot{\boldsymbol{\psi}}(t) = -\mathbf{Q}\mathbf{r}(t) - \mathbf{A}^\top \boldsymbol{\psi}(t), \quad \boldsymbol{\psi}(t_f) = \mathbf{Q}_f \mathbf{r}(t_f). \quad (35)$$

Note that (7) is a strictly convex function of $\mathbf{u}_r(t)$ for all admissible control functions, and the dynamics are linear. Therefore, the conditions obtained from Pontryagin's principle are both necessary and sufficient [28, 29].

Substituting (34) into the state dynamics (6), we have

$$\dot{\mathbf{r}}(t) = \mathbf{A}\mathbf{r}(t) - \mathbf{B}\mathbf{R}^{-1}\mathbf{B}^\top \boldsymbol{\psi}(t), \quad \mathbf{r}(0) = \mathbf{r}_0. \quad (36)$$

Equations (36) and (35) are unified into the following differential equation

$$\begin{bmatrix} \dot{\mathbf{r}}(t) \\ \dot{\boldsymbol{\psi}}(t) \end{bmatrix} = \mathbf{M} \begin{bmatrix} \mathbf{r}(t) \\ \boldsymbol{\psi}(t) \end{bmatrix}, \quad (37)$$

where \mathbf{M} is given by (10). Moreover, the initial and terminal conditions are unified as

$$\begin{bmatrix} \mathbf{I} & \mathbf{0} \\ \mathbf{0} & \mathbf{0} \end{bmatrix} \begin{bmatrix} \mathbf{r}(0) \\ \boldsymbol{\psi}(0) \end{bmatrix} + \begin{bmatrix} \mathbf{0} & \mathbf{0} \\ -\mathbf{Q}_f & \mathbf{I} \end{bmatrix} \begin{bmatrix} \mathbf{r}(t_f) \\ \boldsymbol{\psi}(t_f) \end{bmatrix} = \begin{bmatrix} \mathbf{r}_0 \\ \mathbf{0} \end{bmatrix}. \quad (38)$$

The solution of (37) at t_f is given by

$$\begin{bmatrix} \mathbf{r}(t_f) \\ \boldsymbol{\psi}(t_f) \end{bmatrix} = \exp(t_f \mathbf{M}) \begin{bmatrix} \mathbf{r}(0) \\ \boldsymbol{\psi}(0) \end{bmatrix}. \quad (39)$$

Substituting (39) into (38), we obtain

$$\left(\begin{bmatrix} \mathbf{I} & \mathbf{0} \\ \mathbf{0} & \mathbf{0} \end{bmatrix} + \begin{bmatrix} \mathbf{0} & \mathbf{0} \\ -\mathbf{Q}_f & \mathbf{I} \end{bmatrix} \exp(t_f \mathbf{M}) \right) \begin{bmatrix} \mathbf{r}(0) \\ \boldsymbol{\psi}(0) \end{bmatrix} = \begin{bmatrix} \mathbf{r}_0 \\ \mathbf{0} \end{bmatrix}, \quad (40)$$

or equivalently,

$$\left(\begin{bmatrix} \mathbf{I} & \mathbf{0} \\ \mathbf{0} & \mathbf{0} \end{bmatrix} \exp(-t_f \mathbf{M}) + \begin{bmatrix} \mathbf{0} & \mathbf{0} \\ -\mathbf{Q}_f & \mathbf{I} \end{bmatrix} \right) \exp(t_f \mathbf{M}) \begin{bmatrix} \mathbf{r}(0) \\ \boldsymbol{\psi}(0) \end{bmatrix} = \begin{bmatrix} \mathbf{r}_0 \\ \mathbf{0} \end{bmatrix}. \quad (41)$$

Let

$$\exp(-t_f \mathbf{M}) = \begin{bmatrix} \mathbf{C}_{11} & \mathbf{C}_{12} \\ \mathbf{C}_{21} & \mathbf{C}_{22} \end{bmatrix}. \quad (42)$$

Multiplying both sides of (41) by $\begin{bmatrix} \mathbf{I} & -\mathbf{C}_{12} \\ \mathbf{0} & \mathbf{I} \end{bmatrix}$, we get

$$\begin{bmatrix} \mathbf{C}_{11} + \mathbf{C}_{12}\mathbf{Q}_f & \mathbf{0} \\ -\mathbf{Q}_f & \mathbf{I} \end{bmatrix} \exp(t_f \mathbf{M}) \begin{bmatrix} \mathbf{r}(0) \\ \boldsymbol{\psi}(0) \end{bmatrix} = \begin{bmatrix} \mathbf{r}_0 \\ \mathbf{0} \end{bmatrix}, \quad (43)$$

or equivalently,

$$\begin{bmatrix} \mathbf{C}_{11} + \mathbf{C}_{12}\mathbf{Q}_f & \mathbf{0} \\ -\mathbf{Q}_f & \mathbf{I} \end{bmatrix} \begin{bmatrix} \mathbf{r}(t_f) \\ \boldsymbol{\psi}(t_f) \end{bmatrix} = \begin{bmatrix} \mathbf{r}_0 \\ \mathbf{0} \end{bmatrix}. \quad (44)$$

Substituting (42) into (9) yields

$$\mathbf{H}(t_f) = \mathbf{C}_{11} + \mathbf{C}_{12}\mathbf{Q}_f. \quad (45)$$

Thus, (43) is rewritten as

$$\begin{bmatrix} \mathbf{H}(t_f) & \mathbf{0} \\ -\mathbf{Q}_f & \mathbf{I} \end{bmatrix} \begin{bmatrix} \mathbf{r}(t_f) \\ \boldsymbol{\psi}(t_f) \end{bmatrix} = \begin{bmatrix} \mathbf{r}_0 \\ \mathbf{0} \end{bmatrix}. \quad (46)$$

From (46), we have

$$\begin{aligned} \begin{bmatrix} \mathbf{r}(t_f) \\ \boldsymbol{\psi}(t_f) \end{bmatrix} &= \begin{bmatrix} \mathbf{H}(t_f) & \mathbf{0} \\ -\mathbf{Q}_f & \mathbf{I} \end{bmatrix}^{-1} \begin{bmatrix} \mathbf{r}_0 \\ \mathbf{0} \end{bmatrix} = \begin{bmatrix} \mathbf{H}^{-1}(t_f) & \mathbf{0} \\ \mathbf{Q}_f\mathbf{H}^{-1}(t_f) & \mathbf{I} \end{bmatrix} \begin{bmatrix} \mathbf{r}_0 \\ \mathbf{0} \end{bmatrix} \\ &= \begin{bmatrix} \mathbf{H}^{-1}(t_f)\mathbf{r}_0 \\ \mathbf{Q}_f\mathbf{H}^{-1}(t_f)\mathbf{r}_0 \end{bmatrix} = \begin{bmatrix} \mathbf{I} \\ \mathbf{Q}_f \end{bmatrix} \mathbf{H}^{-1}(t_f)\mathbf{r}_0, \end{aligned} \quad (47)$$

Substituting (47) into (39) and rearranging it, we get

$$\begin{bmatrix} \mathbf{r}(0) \\ \boldsymbol{\psi}(0) \end{bmatrix} = \exp(-t_f\mathbf{M}) \begin{bmatrix} \mathbf{I} \\ \mathbf{Q}_f \end{bmatrix} \mathbf{H}^{-1}(t_f)\mathbf{r}_0. \quad (48)$$

Substituting (48) into the solution of (37) at t yields

$$\begin{bmatrix} \mathbf{r}(t) \\ \boldsymbol{\psi}(t) \end{bmatrix} = \exp(t\mathbf{M}) \begin{bmatrix} \mathbf{r}(0) \\ \boldsymbol{\psi}(0) \end{bmatrix} = \exp((t-t_f)\mathbf{M}) \begin{bmatrix} \mathbf{I} \\ \mathbf{Q}_f \end{bmatrix} \mathbf{H}^{-1}(t_f)\mathbf{r}_0. \quad (49)$$

From (49), we have

$$\mathbf{r}(t) = \begin{bmatrix} \mathbf{I} & \mathbf{0} \end{bmatrix} \exp((t-t_f)\mathbf{M}) \begin{bmatrix} \mathbf{I} \\ \mathbf{Q}_f \end{bmatrix} \mathbf{H}^{-1}(t_f)\mathbf{r}_0. \quad (50)$$

Using the notation in (9), we get (8). This concludes the proof. \square

References

- [1] P. Petráček, V. Krátký, M. Petrlík, T. Báča, R. Kratochvíl, and M. Saska, “Large-scale exploration of cave environments by unmanned aerial vehicles,” *IEEE Robotics and Automation Letters*, vol. 6, no. 4, pp. 7596–7603, 2021.
- [2] C. O. Barcelos, L. A. Fagundes-Júnior, D. K. D. Villa, M. Sarcinelli-Filho, A. P. Silvatti, D. C. Gandolfo, and A. S. Brandão, “Robot formation performing a collaborative load transport and delivery task by using lifting electromagnets,” *Applied Sciences*, vol. 13, no. 2, p. 822, 2023.

- [3] T. Uzakov, T. P. Nascimento, and M. Saska, "UAV vision-based nonlinear formation control applied to inspection of electrical power lines," in Proc. Int. Conf. Unmanned Aircraft Systems (ICUAS), 2020, pp. 1301–1308.
- [4] M. Saska, D. Hert, T. Baca, V. Kratky, and T. Nascimento, "Formation control of unmanned micro aerial vehicles for straitened environments," Autonomous Robots, vol. 44, no. 6, pp. 991–1008, 2020.
- [5] Y. Alqudsi, M. Makaraci, A. Kassem, and G. El-Bayoumi, "A numerically-stable trajectory generation and optimization algorithm for autonomous quadrotor UAVs," Robotics and Autonomous Systems, vol. 170, p. 104532, 2023.
- [6] N. A. Letizia, B. Salamat, and A. M. Tonello, "A novel recursive smooth trajectory generation method for unmanned vehicles," IEEE Transactions on Robotics, vol. 37, no. 5, pp. 1792–1805, 2021.
- [7] J. Wang and M. Xin, "Integrated optimal formation control of multiple unmanned aerial vehicles," IEEE Transactions on Control Systems Technology, vol. 21, no. 5, pp. 1731–1744, 2013.
- [8] Y. Huang, W. Liu, B. Li, Y. Yang, and B. Xiao, "Finite-time formation tracking control with collision avoidance for quadrotor UAVs," Journal of the Franklin Institute, vol. 357, no. 7, pp. 4034–4058, 2020.
- [9] Z. Du, H. Zhang, Z. Wang, and H. Yan, "Model predictive formation tracking-containment control for multi-UAVs with obstacle avoidance," IEEE Transactions on Systems, Man, and Cybernetics: Systems, early access, 2024.
- [10] B. Li, W. Gong, Y. Yang, and B. Xiao, "Distributed fixed-time leader-following formation control for multi-quadrotors with prescribed performance and collision avoidance," IEEE Transactions on Aerospace and Electronic Systems, vol. 59, no. 5, pp. 7281–7294, 2023.
- [11] R. Chai, A. Savvaris, A. Tsourdos, S. Chai, and Y. Xia, "Trajectory optimization of space maneuver vehicle using a hybrid optimal control solver," IEEE Transactions on Cybernetics, vol. 49, no. 2, pp. 467–480, 2019.
- [12] B. Sabetghadam, R. Cunha, and A. Pascoal, "A distributed algorithm for real-time multi-drone collision-free trajectory replanning," Sensors, vol. 22, no. 5, p. 1855, 2022.
- [13] H. Li, H. Chen, and X. Wang, "Collision-free formation generation and tracking of unmanned aerial vehicles based on physicomimetics approach," Asian Journal of Control, vol. 25, no. 4, pp. 2752–2775, 2023.
- [14] X. Ai and J. Yu, "Flatness-based finite-time leader-follower formation control of multiple quadrotors with external disturbances," Aerospace Science and Technology, vol. 92, pp. 20–33, 2019.
- [15] H. Liu, T. Ma, F. L. Lewis, and Y. Wan, "Robust formation trajectory tracking control for multiple quadrotors with communication delays," IEEE Transactions on Control Systems Technology, vol. 28, no. 6, pp. 2633–2640, 2020.

- [16] Z. Shi, J. He, T. Wang, C. Zhou, and J. Guo, “Optimal formation control and collision avoidance in environment with multiple rectangle obstacles,” Journal of the Franklin Institute, vol. 355, no. 15, pp. 7626–7642, 2018.
- [17] K. Lee, C. Park, and S. Y. Park, “Near-optimal continuous control for spacecraft collision avoidance maneuvers via generating functions,” Aerospace Science and Technology, vol. 62, pp. 65–74, 2017.
- [18] D. Mellinger and V. Kumar, “Minimum snap trajectory generation and control for quadrotors,” in Proc. IEEE Int. Conf. Robotics and Automation (ICRA), 2011, pp. 2520–2525.
- [19] A. E. Bryson, “Optimal control–1950 to 1985,” IEEE Control Systems Magazine, vol. 16, no. 3, pp. 26–33, 1996.
- [20] J. T. Betts, Practical Methods for Optimal Control and Estimation Using Nonlinear Programming, SIAM, 2010.
- [21] X. Ai and J. Yu, “Fixed-time trajectory tracking for a quadrotor with external disturbances: A flatness-based sliding mode control approach,” Aerospace Science and Technology, vol. 89, pp. 58–76, 2019.
- [22] H. Du, W. Zhu, G. Wen, Z. Duan, and J. Lü, “Distributed formation control of multiple quadrotor aircraft based on nonsmooth consensus algorithms,” IEEE Transactions on Cybernetics, vol. 49, no. 1, pp. 342–353, 2019.
- [23] L. E. Beaver and A. A. Malikopoulos, “Optimal control of differentially flat systems is surprisingly easy,” Automatica, vol. 159, p. 111404, 2024.
- [24] H. B. Jond and V. Nabiyev, “On the finite horizon Nash equilibrium solution in the differential game approach to formation control,” Journal of Systems Engineering and Electronics, vol. 30, no. 6, pp. 1233–1242, 2019.
- [25] H. B. Jond, V. Nabiyev, N. Özmen, and D. Lukáš, “Existence of Nash equilibrium in differential game approach to formation control,” International Journal of Robotics and Automation, vol. 33, p. 206, 2018.
- [26] D. M. Stipanović, P. F. Hokayem, M. W. Spong, and D. D. Šiljak, “Cooperative avoidance control for multiagent systems,” Journal of Dynamic Systems, Measurement, and Control, vol. 129, no. 5, pp. 699–707, 2007.
- [27] V. Walter, N. Staub, A. Franchi, and M. Saska, “UVDAR system for visual relative localization with application to leader–follower formations of multirotor UAVs,” IEEE Robotics and Automation Letters, vol. 4, no. 3, pp. 2637–2644, 2019.
- [28] J. C. Engwerda, “On the open-loop Nash equilibrium in LQ-games,” Journal of Economic Dynamics and Control, vol. 22, no. 5, pp. 729–762, 1998.
- [29] U. Ledzewicz and H. Schättler, “Pitfalls in applying optimal control to dynamical systems: An overview and editorial perspective,” Discrete and Continuous Dynamical Systems-B, vol. 27, no. 11, pp. 6711–6722, 2022.